**REVISION 3**

# Phosphorus partitioning between olivine and melt: An experimental study in the system $Mg_2SiO_4$-$Ca_2Al_2Si_2O_9$-$NaAlSi_3O_8$-$Mg_3(PO_4)_2$.

Thomas B. Grant[*1,2] and Simon C. Kohn[1]

[1]Department of Earth Sciences, University of Bristol, Queens Rd., Bristol, BS8 1RJ, United Kingdom

[2]Institut für Geologische Wissenschaften, Freie Universität Berlin, Malteserstrasse, 74-100 12249 Berlin, Germany

## Abstract

The partitioning of phosphorus between olivine and melt was measured by conducting partitioning experiments within the system $Mg_2SiO_4$-$Ca_2Al_2Si_2O_9$-$NaAlSi_3O_8$-$Mg_3(PO_4)_2$, using olivines crystallized with cooling rates in the range 1°C/hour to 10°C/hour. Partition coefficients, $D_P^{ol/melt}$, vary from 0.05 to 1.41 and are strongly influenced by melt composition, with high partition coefficients observed for more polymerized melts. Correlations between elemental abundances in the olivines demonstrate that phosphorus substitutes on a near one for one basis for Si, charge-balanced by a vacancy in Mg and no correlation between P and Al concentration in the olivine was observed. A complete understanding of the controls on $D_P^{ol/melt}$ is required to model quantitatively the zoning of P in olivine that has recently been shown to be a common feature of igneous olivine crystals. The strong melt compositional dependence observed in this study implies that both changing concentrations of P in the melt during fractionation, and changing values of $D_P^{ol/melt}$ can contribute to core-to-rim variations in P when the surface composition of a growing olivine crystal is in equilibrium with the melt. The common observation of zones in natural olivines where high P is correlated with high Al and Cr must be explained by processes other than equilibrium growth and, as suggested previously, such zones are probably related to solute trapping during episodes of rapid growth.

Key words: Phosphorus, Olivine, Partitioning, Zoning, Experiemental petrology

## INTRODUCTION

The role of phosphorus in primary magmatic melts has gained significant attention over the last thirty years due to its impact on phase equilibria (particularly the size of liquid immiscibility fields) (Kushiro 1975, Toplis et al 1994), its preference for basic melts over acid (more evolved) melts, and its higher partition coefficient in olivine relative to pyroxene (Mallmann et al 2009, Millman-Barris et al 2008, Konzett et al., 2012). More recently, a wide range of phosphorus zoning features have been discovered within olivine phenocrysts from a variety of sources including basalts, andesites, dacites, komatiites, chondrites and experimentally produced olivines (Millman-Barris et al 2008, Spandler et al 2007, Mallmann et al 2009, McCanta et al 2008, McCanta et al 2009) and even metasomatised peridotites (Mallmann et al., 2009). The reproducibility of these findings by a number of different authors and for different magmatic conditions suggest that phosphorus zoning is very common. This is largely due to the slow diffusion rate of P (Spandler et al 2007) within olivine, which makes zoning difficult to erase even under long magmatic residence times and high temperatures. Many of the zoning patterns previously described have been attributed to rapid growth kinetics coupled with the slow diffusivity of P in melts leading to the process of solute trapping (Reitano et al 1994). This occurs when the rate of crystal growth exceeds the rate at which phosphorus can diffuse through the melt away from the crystal / liquid boundary layer. The net effect is that it is generally difficult to produce olivines that are in equilibrium with the melt with respect to P and once created, P-zones are difficult to erase.

Whilst many of these zoning features have been attributed to disequilibrium kinetics, the value of the equilibrium phosphorus partition coefficient is somewhat poorly known. To have any hope of quantitatively exploiting phosphorus zoning in olivine, well constrained values for the partition coefficient, and its sensitivity to parameters such as pressure, temperature, melt concentration and volatile fugacities are required. The focus of the research presented here is to provide experimentally produced coefficients for the partitioning of phosphorus between olivine and melt ($D_P^{ol/melt}$) over a range of compositions and temperatures with the potential application to natural magmatic systems which develop P zoned olivine.

There are currently two sources of data on $D_P^{ol/melt}$; experimental mineral-melt partitioning studies and partition coefficients derived from natural mineral-melt pairs. The available data are summarized in table 1. The reported values of $D_P^{ol/melt}$ vary significantly from around 1

down to about 0.02. The lowest figures are thought to represent values closest to equilibrium, and McCanta et al (2008) and Millman-Barris et al (2008) both noted that the equilibrium partition coefficient for their experiments should be <0.1. The higher values have been attributed to non-equilibrium partitioning via processes such as solute trapping (Reitano et al 1994) during rapid growth. Scenarios that can generate non-equilibrium, apparent partition coefficients are detailed by Albarede and Bottinga (1972).

A further consideration is the mechanism by which $P^{5+}$ is incorporated into olivine. It is widely accepted that, due to its similar charge and ionic radius P will dominantly substitute for $Si^{4+}$ into the tetrahedral site. However, the extra positive charge of $P^{5+}$ compared with $Si^{4+}$ must be balanced, either: i) by the creation of vacancies on M sites (Agrell et al 1998, Tropper et al, 2004 and Boesenberg and Hewins, 2010); ii) by a charge coupled substitution of a monovalent ion such as Li, Na (Mallmann et al 2009) or H (Witt-Eickschen and O'Neill, 2005) replacing a divalent cation on an M site or iii) by a charge coupled substitution of a trivalent cation such as Al or Cr (Millman-Barris et al, 2008; McCanta et al, 2008) replacing $Si^{4+}$ on a T site. These mechanisms are represented by the following reactions:

$$Mg_2SiO_{4(ol)} + ½\ P_2O_{5(m)} \Rightarrow Mg_{1.5}[]_{0.5}PO_{4(ol)} + ½\ MgO_{(m)} + SiO_{2(m)} \quad (1)$$

$$Mg_2SiO_{4(ol)} + ½\ P_2O_{5(m)} + ½\ Li_2O_{(m)} \Rightarrow MgLiPO_{4(ol)} + MgO_{(melt)} + SiO_{2(m)} \quad (2)$$

$$Mg_2SiO_{4(ol)} + ¼\ P_2O_{5(m)} + ¼\ Al_2O_{3(m)} \Rightarrow Mg_2Al_{0.5}P_{0.5}O_{4(ol)} + SiO_{2(m)} \quad (3)$$

The different substitution reactions would give different predictions of the covariance of element concentrations in olivine. All reactions would predict an inverse correlation between P and Si in olivine, but for the system studied here, (2) would predict a correlation between P and Na and (3) would predict a correlation between P and Al in olivine. In this study we will provide new experimental data on the equilibrium values of $D_P^{ol/melt}$ and its melt compositional dependence, determine the mechanism of P incorporation and discuss the relevance of the data to non-equilibrium incorporation of P during rapid crystal growth.

## EXPERIMENTAL METHODS

The starting compositions chosen for this study were guided by the phase diagram for the Fo-An-Ab system (Schairer and Yoder, 1966), but in the system $Mg_2SiO_4$-$Ca_2Al_2Si_2O_9$-$NaAlSi_3O_8$. Initially two sets of starting compositions were produced, shown as the filled symbols in Figure 1. The compositions of all starting materials are given in Table 2. Starting materials in the system $Mg_2SiO_4$-$Ca_2Al_2Si_2O_9$-$NaAlSi_3O_8$-$Mg_3P_2O_8$ were made by preparing mixtures of forsterite, albite and $Ca_2Al_2Si_2O_9$ compositions. Each end-member composition was prepared by weighing and mixing the respective oxide and carbonate in the correct molar proportions. Then each composition was heated at about 1000°C to decarbonate and form a homogenous mixture before being ground into a fine powder using an agate pestle and mortar. Half of a gram of each experimental composition was then produced by accurately weighing the required mass of each end member normalized to 98% to account for the addition of 2% $P_2O_5$. The source of the $P_2O_5$ was trimagnesium phosphate octahydrate ($Mg_3P_2O_8 \cdot 8H_2O$); the mass of the water in this compound was accounted for in measured amounts of the starting materials and later removed by dehydrating each starting composition.

The choice of 2% $P_2O_5$ in starting materials was made to facilitate analysis by electron probe microanalysis but leads to phosphorus concentrations in the experimental products that are much higher than is normally found in naturally occurring mafic terrestrial melts not saturated in apatite (although some meteorite samples have olivine with high P contents). It is also higher than previously conducted experiments whose compositions contained 0.24% (McCanta et al 2008) or 0.16-1.18% $P_2O_5$ (Millman-Barris et al 2008). A further set of starting compositions were therefore produced to test the effect of differing amounts of $P_2O_5$ (compositions 11-13, used in samples 21-23). These were based on composition 3, but with $P_2O_5$ concentrations of 1%, 0.6% and 0.3%. In order for direct comparisons to be made, additional MgO was added to the starting compositions to account for the lower amounts of trimagnesum phosphate used.

Starting materials were packed into 3mm diameter and 8-10 mm long platinum capsules that had been sealed at one end using a PUK3 arc welder and then the capsules were crimped at the open end using a pair of pliers. The capsules were dried in a box furnace at around 600-900°C for 30-60 minutes to release any water adsorbed onto the powdered starting materials and then the crimped end was welded shut. Completely sealed capsules were used to avoid

the loss of volatile components during the long, high-temperature runs. Platinum wire was used to wrap around the capsules and to suspend them at the hotspot of a vertical 1 atmosphere furnace. The furnace was already at the starting temperature of the run when the samples were introduced and the position of the hotspot had been previously calibrated for each run temperature. The samples were all within about 10 mm of a thermocouple bead. All experiments were drop quenched into water. Full details of the run conditions, composition numbers and sample numbers are given in table 3. It is worth noting that the cooling rates (1, 5, or 10º/hr) of the experiments presented here are up to an order of magnitude lower than those of previous experimental runs by other authors whose cooling rates typically ranged from 5º. 10º, and 15ºC/hr in McCanta et al (2008) and 15º or 30ºC/hr in Millman-Barris et al (2008). After quenching, samples were removed from their capsules and mounted in 1 inch aluminum rings using epoxy resin. These were then ground and polished to a 1µm finish using diamond-impregnated pads.

Samples were imaged using a JEOL JXA 8600 SEM, and quantitative analysis of olivine and glass phases was performed using a CAMECA SX100 electron microprobe (EPMA). Olivine analysis was performed using an accelerating voltage of 20keV, a beam current of 100 nA and a 1µm focused beam to maximize the analytical sensitivity for P. P counts were measured simultaneously on 3 spectrometers, each with a PET crystal, giving a total counting time of 720s on peak and 720s on background. Al was measured with 120s on peak and background, Ca with 240s on peak and background and Mg, Si and Na with 10s on peak and background. In contrast, for the glasses, an accelerating voltage of 20keV, a beam current of 2-4 nA and a defocused beam (about 12µm in diameter) was used to minimize beam damage to the sample. Counting times were 30s (peak and background) for P and Ca and 10s for all other elements. The standards used were St. John's Island olivine (Mg in olivine and glass; Si in olivine), Amelia albite (Na), Eifel sanidine (Al), wollastonite (Si in glass) and Durango apatite (Ca, P).

A limited number of additional analyses were performed using a JEOL JXA 8530F FEG (field emission gun) EPMA. These analyses were focused on samples 1 and 6, the samples with this highest measured $D_P^{ol/melt}$ for the high temperature and low temperature 1°C/hour series respectively and sample 2. Sample 6 in particular was judged to be the one that was most likely to be affected by processes such as enrichment or depletion in P in the melt

adjacent to growing crystals, olivine rims with compositions different from cores and other experimental difficulties. Therefore, several high-spatial-resolution traverses across crystal/melt interfaces were measured and detailed investigations of the heterogeneity of olivine rims were performed. A variety of analytical conditions were used for the different analyses, but the emphasis was on spatial resolution rather than counting statistics. The accelerating voltage was 8-10 keV and the beam current was 9-50 nA. Under the conditions used the analysed volume was always less than 1 $\mu m^3$ as determined using the CASINO software (Hovington et al., 1997) for Monte Carlo simulation of the electron-sample interaction (personal communication, Dr Ben Buse) and fluorescence problems were negligible.

A separate set of five isothermal experiments with a duration of 167 hours were performed at 1420°C to avoid the potential complexities of crystal growth during cooling ramp experiments. However, the crystals were too small to be analyzed without contamination by glass, so the results of this set of experiments are not reported here. Furthermore, 2 of the 5 samples from this series were found to have very low bulk phosphorus concentrations. The phosphorus loss is probably due to failure of the capsule weld and subsequent volatilization of $P_2O_5$ (e.g. Welch and Gutt, 1961; Levin and Roth, 1970). The same problem of phosphorus loss was observed in one other sample from the 1400°C/5°C per hour cooling rate series. We therefore do not report any data for that sample

## RESULTS

### Phosphorus partitioning data

All samples contained olivine crystals within a homogenous glass, and no other phases were seen in any sample. Olivine crystals were typically euhedral and rarely showed any textures diagnostic of rapid growth, although some crystals in the faster cooling-rate experiments included small melt pools within euhedral outer crystal edges. Olivine composition measurements were predominantly taken as traverses across randomly oriented sections in the polished samples, and the glass compositions were taken at random locations and also as traverses away from crystals. Averages of all these points were taken for each sample and are given in table 4. Glass compositions for samples 1-10 (all of which cooled at 1°C/hour) are

plotted as open symbols in Figure 1, together with the compositions of the starting materials for these samples (filled symbols). The compositions are consistent with crystallization of around 10% forsterite from each starting composition, and the glass compositions represent the 1400°C and 1270°C isotherms in the modified Fo-An-Ab system used here. The average olivine and glass compositions for each sample were used to calculate the partition coefficients for each sample and these are also given in Table 4. The lowest observed value of $D_p^{ol/melt}$ was 0.05, obtained for sample 5 (An-rich melt, final temperature of 1400°C, cooling rate of 1°/hr), and the highest value of 1.41 was observed in sample 6 (Ab-rich melt, final temperature of 1270°C, cooling rate of 1°/hr). It is obvious from these two points alone that there is a significant effect of the melt composition and temperature on partitioning of P even when the cooling rate is the same (and very slow). The trend of increasing partition coefficient with increasing albite content / decreasing forsterite content of the melt and at lower temperatures is consistent across all the different experimental runs. An additional trend that can be seen is that there is a slight increase in the partition coefficient with increasing cooling rate, although this is far less pronounced than the variations across different compositions under the same cooling rate. Whereas some of the data obtained in this study are comparable to those from previous published studies (Adam and Green 2006; Anderson and Greenland 1969; Brunet and Chazot 2001; Beck et al. 2006) some of the new values are much higher. An analysis of whether these samples are equilibrated or not will be presented in the discussion section.

Nearly all observed olivine crystals were, to some extent, zoned with respect to P. Typical core to rim traverses are shown in figure 2. A number of features were documented, including P concentrations that rise smoothly towards the rims, P concentrations that drop smoothly towards the rims and jumps in P concentration leading to either symmetrical or asymmetrical low or high P zones. Many of these features are comparable to those described in the literature (Millman-Barris et al 2008, McCanta et al 2009, McCanta et al 2008). The smoothly increasing P concentrations can be explained by some combination of changing P concentration in the melt as crystallization progresses (Rayleigh distillation) combined with increasing $D_P$ as the melts become more polymerized by the removal of the forsterite component in the melt. Similarly, smooth decreases in P concentration are consistent with changing P concentration in the melt for samples with $D_P > 1$. The jumps in P concentration could be related to sector zoning which was observed in some crystals using cathodoluminescence. In addition, phenomena such as solute trapping resulting from the

interplay between P diffusivity in the melt, $D_P$ and growth rate may play some role, especially at the faster cooling rates.

The values of $D_P^{ol/melt}$ reported in table 4 are, in some cases, surprisingly high, therefore our approach of calculating $D_P$ for each sample using a simple average of all P analyses in all olivine crystals for a given sample needs further consideration. It could be argued: i) that a better measure of equilibrium P concentration in olivine is the P concentration at the rims of crystals; and ii) that the melt adjacent to olivine crystals could be enriched in P (because of slow diffusion in the melt. To investigate these two potential problems with our data, two samples with the highest $D_P^{ol/melt}$ for the high temperature, 1°C/hour series (sample 1 and 2) and one from the low temperature, 1°C/hour series (sample 6) were studied in more detail by FEG EPMA. The counting statistics are inferior to the standard EPMA, and calibration is more difficult, so we do not include any of the data in the calculation of $D_P^{ol/melt}$ but the superior spatial resolution of the FEG instrument allows the details of P distribution around crystal/melt interfaces to be studied in more detail. The two questions addressed with the FEG probe were: (i) is there a zone of P enrichment or depletion in the melt adjacent to growing crystals? Such a zone could result from crystal growth rates exceeding P diffusion rates in the melt and would have implications for measured $D_P^{ol/melt}$ and (ii) is there a systematic difference in olivine rim compositions compared with olivine core compositions? Figure 3 shows a data set for sample 2 from the FEG probe that includes a backscattered electron image, Mg, Si and P X-ray maps and a traverse generated from the P X-ray map that shows the relative count rates as the rim is approached and over the olivine/melt interface. The map and profile clearly show that P concentration at the rim of the olivine is close to that of the interior of the olivine and that there is absolutely no trace of zoning in the glass adjacent to the crystal. Figure 4 shows a high-resolution (FEG probe) line scan across an olivine crystal in sample 6. This is the sample with the highest partition coefficient in this study, and hence the one that is most likely to display non-equilibrium features. As expected (c.f. figure 2d) there is significant core-to-rim zoning, but what was not expected was the jump in P concentration and the complex profile near the rim. We do not have a satisfactory explanation for these effects, but these measurements do show that using rim compositions alone to obtain the P concentration of olivine in equilibrium with melt is unlikely to be successful. As a direct test of this idea we used the FEG probe to measure the composition of 48 points near the rim of several different olivines in sample 1 and 11 points near rims on sample 6. For sample 1 we obtained a mean $P_2O_5$ concentration of 0.766 wt% with a standard

deviation of 0.213 wt%. This compares with our preferred method of averaging all CAMECA EPMA analyses of olivines for that sample of 0.961 wt% with a standard deviation of 0.073 wt% (see Table 4). Thus in this case the rims compositions are more variable than the olivines as a whole, and the mean values, although a little different, are within the uncertainties. For sample 6 we obtained a mean of 2.945±0.703 wt% for olivine rims using the FEG probe and 2.896±0.418 wt% using the overall olivine compositions from the CAMECA EPMA data (Table 4). The explanation for the variation in rim compositions is probably that different crystals nucleate at different times during the run, then grow at different rates and while some will continue to grow throughout the run, some may dissolve during the process of surface energy minimisation, thus different crystals are at different stages of evolution at the time of quenching. In summary the detailed analyses using the FEG probe confirm that using the overall average olivine composition from the CAMECA data set is the best approximation to the equilibrium olivine composition and that there is no measurable inhomogeneity in the glass close to olivine crystals.

**Mechanisms of phosphorus incorporation in olivine**

Figure 5 shows the correlations between P and other elements in samples from the two 1°C/hour series, expressed as the number of cations per four oxygens. In each case the expected correlation for each of reactions 1, 2 and 3 is shown. For Si the slope is exactly that expected for both reactions 1 and 2; the offset (1% of the value for the number of Si per 4O) is almost certainly a consistent, systematic, analytical error arising from the analytical conditions that were optimized for sensitive determination of low concentrations of P rather than accurate measurements on major elements. For Mg, the slope matches equation 1, with an offset that can be explained in the same way as the Si plot, but for Al and Na there is no agreement with the expected trends for reactions 3 and 2 respectively. For Al, the P concentration seems to be essentially independent of Al concentration, whereas for Na the increasing P concentration as a function of increasing Na concentration is simply a consequence of a correlation between albite and forsterite concentrations in the melt. Thus our data clearly point to incorporation of P in olivine according to reaction 1 in agreement with the observations of Agrell et al. (1998), Tropper et al, (2004) and Boesenberg and Hewins, (2010). It is significant to note that the lack of correlation between the concentration of P and Al in the olivine crystals is in contrast to the observations of Millman-Barris et al (2008) and McCanta et al (2008). The correlation of P with Al and Cr observed in the earlier

studies is likely to be a reflection of the disequilibrium rapid-growth conditions in both experiments and naturally occurring phenocrysts.

**Partitioning data for other elements**

Although this study was aimed at elucidating the phosphorus partitioning behavior, the Ca, Na and Al concentrations of both olivine and melt were also measured, allowing partition coefficients for these elements to be determined. $D_{Ca}$ is found to be $2.6\pm0.3 \times 10^{-2}$, with no systematic trends as a function of temperature, melt composition or cooling rate being apparent. This is contrary to the data summarized in Libourel (1999) where $D_{Ca}$ increases significantly with the sodium content of the melt. However, in the case of Watson (1977) and for the majority of the glasses presented here, the sodium effect is cancelled out by the anti correlation of CaO and $Na_2O$ (Libourel, 1999). Our $D_{Ca}$ values are consistently around a factor of 2 lower than those predicted by Libourel (1999). This could be due to the creation of vacancies in the M sites of olivine by the incorporation of P, or partly due to the stoichiometry of the melts, having no excess Ca. Our values are fairly consistent with those of Adam and Green (2006) ($1.3 \times 10^{-2}$ - $2.4 \times 10^{-2}$), Beattie (1994) ($1.92 \times 10^{-2}$ - $3.75 \times 10^{-2}$), Dunn (1987) ($3.4 \times 10^{-2}$) and Ohtani et al (1989) ($2 \times 10^{-2}$) despite the varying range of melt compositions and conditions. $D_{Na}$ has a value of $4.8\pm1.4 \times 10^{-3}$ in our experiments, similar to previous measurements of $3.1 \times 10^{-3}$ (Borisov et al., 2008) and $1.5 \times 10^{-4}$ to $3 \times 10^{-2}$ (Grant and Wood 2010). The very low concentrations of Na in olivine make it difficult to observe any significant trends in the data. $D_{Al}$ is the only element of the three where clear trends can be observed as a function of composition. $D_{Al}$ has a range of $5 \times 10^{-3}$ to $1.5 \times 10^{-2}$ with an average of $8.5\pm3.0 \times 10^{-3}$, which is similar to the values found by Grant and Wood (2010) and the lowest values given by Millman-Barris et al (2008). For our experiments with the higher cooling rates the uncertainty on Al concentration in olivine is larger, which was also noted by Pack and Palme (2003). Pack and Palme (2003) did not find any correlation between cooling rate and Al content but in their study the incorporation of Al became notably more irregular at higher cooling rates. The 1°C/hour samples show interesting trends, particularly the 1400°C samples which show a progressive reduction in $D_{Al}$ with increasing albite component in the melt and decreasing NBO/T. In summary, the olivines in the present study tend to have partition coefficients for elements other than P that agree well with the literature, providing further indirect evidence that our experiments represent conditions close to equilibrium, particularly for the 1°C/hour samples.

## DISCUSSION

### Attainment of equilibrium

The original motivation for the present study was the observation that very fine scale zoning can be observed in natural olivines, apparently preserved through later processes by the extraordinarily slow diffusion of P in olivine. This slow diffusion rate poses a problem for experimental studies as once olivine has crystallized with a particular phosphorus concentration it is very difficult to re-equilibrate it. Reversal experiments are therefore not feasible. In this study we use the following criteria to indicate close approach to equilibrium (while acknowledging that true equilibrium is not possible in this system): i) near-constant P concentration across measured profiles within individual olivines; ii) the same P concentrations in different olivine crystals in the same sample; iii) homogeneous glass compositions, even close to olivine crystals; iv) consistent trends in partition coefficients as a function of T and/or melt composition; v) constant partition coefficients as a function of cooling rate. In all samples the glasses are effectively homogeneous, satisfying criterion (iii). The range of olivine compositions observed for each sample (a combination of criteria (i) and (ii)) are reflected in the quoted standard deviations in table 4, and are clearly lower for the 1400°C and 1°C/hour samples than the equivalent 5°C/hour and 10°C/hour samples. As illustrated in Figure 2 this is partly because the zoning of individual crystals is less pronounced than in the more rapidly-cooled samples, but more strongly influenced by the smaller distribution in P concentrations between crystals. Finally for all the 1400°C samples, there is rather little variation in $D_P$ as a function of cooling rate for each bulk composition, despite the signs of disequilibrium in the 5°C/hour and 10°C/hour samples, therefore we can accept the values of $D_P$ for the 1°C/hour series as reliable, near-equilibrium partition coefficients. For the 1270°C series we have only one cooling rate, so criterion (v) cannot be applied. As the P concentration in olivine is much higher in this series, the standard deviations are of course larger, but even as a proportion of the P concentration the standard deviations are on average 50% larger than the standard deviations for the 1400°C and 1°C/hour series.

### The effect of melt composition on $D_P^{ol/melt}$

Several previous studies of trace element partitioning in simple systems have shown that melt composition plays a role in controlling partition coefficients, and systematic relationships between $D_i$ and NBO/T (the number of non-bridging oxygens per tetrahedral cation) have been observed (e.g. Mysen and Virgo, 1980, Kohn and Schofield, 1994, Toplis and Corgne, 2002). Other studies have preferred simpler formulations such as $X_{SiO2}$ (e.g. Evans et al., 2008). Figure 6 shows $\ln D_P$ plotted as a function of both NBO/T and $X_{SiO2}$. Both plots show a reasonable linear correlation for samples from the 1°C/hour series (filled symbols) and even if the 5°C/hour and 10°C/hour data are included there is a clear overall trend, although the more rapidly cooled samples have generally slightly higher values of $D_P$. The very strong effect of melt composition on $D_P$ is consistent with the well-known melt compositional controls on apatite solubility in melts (e.g. Watson, 1979, Wolf and London, 1994). There is an excellent correlation between $D_P$ from this study and apatite solubility calculated according to the model of Harrison and Watson (1984), with increasing $D_P$ correlating with decreasing predicted apatite solubility. However, the slope is relatively shallow, so that the predicted apatite solubility varies by a factor of 3, whereas the observed values of $D_P$ vary by a factor of 28. It should be noted however that the Harrison and Watson (1984) model only includes wt% $SiO_2$ and temperature as variables, whereas factors such as ASI probably also play a role in the extreme behavior observed here. The complexities in component mixing in the melt will be reflected in extreme activity coefficients for $P_2O_5$ in high-silica, Ab-rich, highly polymerized melts.

**Effect of P concentration on $D_P$**

One issue that has not yet been addressed in the discussion of the data so far, is whether or not $D_P$ depends on bulk P concentration in the system i.e. whether P partitioning follows Henry's Law behaviour. We cannot unambiguously answer this question, as the three samples with low P concentrations (21, 22 and 23) do seem to have $D_P$ values that are below the regression lines in figure 6. However, the uncertainties in $D_P$ for the samples with low total P concentration may simply be too large to allow a meaningful comparison of the apparent differences in $D_P$ at this level of detail. Further studies of the effect of P concentration on $D_P$ using analytical methods such as laser ablation ICPMS, that are more suited to low concentrations, would be worthwhile. It would be surprising for a lower trace element concentration to lead to a reduced partition coefficient, as most cases of non-Henry's Law behavior show the opposite effect, i.e. partition coefficients are reduced at trace element

concentrations above the Henry's Law limit (e.g. Beattie 1993, Pan et al. 2003, Prowatke and Klemme 2006). Thus we are confident that our partition coefficients can be applied to natural olivine-melt systems, and that the strong melt compositional effect on $D_P$ should be taken into account in interpreting zoning profiles in natural olivine crystals.

**Implications to observed zoning profiles in natural olivine crystals**

The most important finding of this study is that there is a strong melt compositional control on $D_P$ such that an olivine growing in a fractionating igneous system will have a changing $D_P$ as the melt composition evolves. Most basalts and basaltic andesites have NBO/T in the range 1 – 0.5 which, for the melt compositions in the present study, would correspond to a range in $D_P$ of 0.2 to 0.8 (although further work on the effect of different types of melt composition is required). Therefore even if P concentration in a melt is constant, the P concentration of crystallizing olivine in an evolving system could increase substantially as the melt composition evolves to more polymerized, silica-rich compositions. Furthermore the absence of any correlation between P and Al in the olivines grown in this study provides clues on the growth-rate-dependence of the coupled P+Al and P+Cr substitutions. Our data suggest that the observation of a zone with high P concentration but without high Al concentration could imply a local equilibrium between the olivine surface and melt during the growth of that zone. Conversely, the observation of correlated P and Al or Cr in previously published studies of zoned olivines may suggest higher growth rates than those of even our 10°C/hour samples, and a role for solute trapping.

Whatever the reason for variable P concentrations in a growing olivine crystal, we agree with previous suggestions that the extremely slow diffusion of P in olivine (Spandler et al 2007) preserves P zoning profiles and provides a potentially very useful method for studying the early history of magmatic evolution. To take full advantage of this resource, more work is required on the role of mineral surface structure, P diffusion in both olivine and melt, boundary layer enrichment in melts and solute trapping effects and the effect of melt composition, temperature and volatile concentrations on $D_P$. Nonetheless, the equilibrium partitioning data produced in this study lay the foundations for quantitative modeling of the zoning profiles of P in olivine. It is particularly significant that $D_P$ cannot be assumed always to be low (<0.1) or constant, as phosphorus can even become compatible in olivine in some extreme circumstances, such as in the highly polymerized, silica rich melts studied here.

**Acknowledgements.** We thank Dr Stuart Kearns for help and instruction with SEM and EPMA, Dr Ben Buse for working out the optimal conditions and training in FEG EPMA and Profs. Jon Blundy, Steve Sparks and Mike Walter and Drs. Oleg Melnik and Ralf Dohmen for illuminating discussions. We are also grateful to Guil Mallmann, an anonymous reviewer and associate editor Chip Lesher for their thorough work and insights.

## REFERENCES

Adam, G., Green, T. (2006). Trace element partitioning between mica- and amphibole-bearing garnet lherzolite and hydrous basanitic melt: 1. experimental results and the investigation of controls on partitioning behaviour. Contributions to Mineralogy and Petrology, 152, 1-17.

Agrell, S.O., Charnley, N.R., Chinner, G.A. (1998). Phophoran olivine from pine canyon, Piute Co., Utah. Mineralogical Magazine, 62, 265-269.

Albarede, F., Bottinga, Y. (1972). Kinetic disequilibrium in trace element partitioning between phenocrysts and host lava. Geochimica et Cosmochimica Acta, 36, 141-156.

Anderson, A. T., Greenland, L.P. (1969). Phosphorus fractionation diagram as a quantitative indicator of crystallization differentiation of basaltic liquids. Geochimica et Cosmochimica Acta, 33, 493-505.

Beattie, P. (1993). On the occurrence of apparent non-Henry's Law behavior in experimental partitioning studies. Geochimica et Cosmochimica Acta, 57, 47-55.

Beattie, P. (1994). Systematics and energetics of trace-element partitioning between olivine and silicate melts: Implications for the nature of mineral/melt partitioning. Chemical Geology, 117, 57-71

Beck, P., Barrat, J., A., Gillet, Ph., Wadhwa, M., Franchi, I.A., Greenwood, R.,C., Bohn, M., Cotton, J., van de Moortele, B., Reynard, B. (2006). Petrography and Geochemistry of the

chassingite Northwest Africa 2737 (NWA 2737). Geochimica et Cosmochimica Acta, 70, 2127-2139.

Boesenberg, J.S., Hewins, R.H. (2010). An experimental investigation into the metastable formation of phosphoran olivine and pyroxene. Geochimica et Cosmochimica Acta, 74, 1923-1941.

Borisov, A. Pack, A., Kropf, A., Palme H. (2008) Partitioning of Na between olivine and melt: An experimental study with application to the formation of meteoritic $Na_2O$-rich chondrule glass and refractory forsterite grains. Geochimica et Cosmochimica Acta, 72, 5558–5573

Brunet, F., Chazot, G. (2001) Partitioning of phosphorus between olivine, clinopyroxene and silicate glass in a spinel lherzolite xenolith from Yemen. Chemical Geology, 176, 51-72.

Dunn, T. (1987). Partitioning of Hf, Lu, Ti, and Mn between olivine, clinopyroxene and basaltic liquid. Contributions to Mineralogy and Petrology, 96, 476-484.

Evans, T.M., O'Neill, H.St.C., Tuff J. (2008) The influence of melt composition on the partitioning of REEs, Y, Sc, Zr and Al between forsterite and melt in the system CMAS. Geochimica et Cosmochimica Acta, 72, 5708–5721

Foley, S.F., Jacob, D.E. and O'Neill, H. St. C. (2011) Trace element variations in olivine phenocrysts from Ugandan potassic rocks as clues to the chemical characteristics of parental magma. Contributions to Mineralogy and Petrology, 162, 1–20

Grant, K.J., Wood, B.J. (2010) Experimental study of the incorporation of Li, Sc, Al and other trace elements into olivine. Geochimica et Cosmochimica Acta, 74, 2412–2428

Harrison, T.M. and Watson, E.B. (1984) The behavior of apatite during crustal anatexis: equilibrium and kinetic considerations. Geochimica et Cosmochimica Acta, 48, 1467–1477

Hovington, P., Drouin, D. and Gauvin, R. (1997) CASINO: A new Monte Carlo code in C language for electron beam Interaction - Part I: Description of the Program. Scanning, 19 1-14.

Kohn, S.C. and Schofield, P.F. (1994) The importance of melt composition in controlling trace-element behaviour: an experimental study of Mn and Zn partitioning between forsterite and silicate melts. Chemical Geology, 117, 73-87.

Konzett, J., Rhede, D. and Frost, D.J. (2012) The high PT stability of apatite and Cl partitioning between apatite and hydrous potassic phases in peridotite: an experimental study to 19 GPa with implications for the transport of P, Cl and K in the upper mantle. Contributions to Mineralogy and Petrology, 163, 277–296.

Kushiro, I. (1975) On the nature of silicate melt and its significance in magma genesis: regularities in the shift of the liquidus boundaries involving olivine, pyroxene and silica minerals. American Journal of Science, 275, 411-431.

Levin, E.M. and Roth, R.S. (1970) The system niobium pentoxide – phosphorus pentoxide. Journal of Solid State Chemistry, 2, 250-261.

Libourel, G. (1999). Systematics of calcium partitioning between olivine and silicate melt: implications for the melt structure and calcium content of magmatic olivines. Contributions to Mineralogy and Petrology, 136, 63-80.

Mallmann, G., O'Neill, H. St. C., Klemme, S. (2009). Heterogenous distribution of phosphorus in olivine from otherwise well-equilibrated spinel peridotite xenoliths and its implications for the mantle geochemistry of lithium. Contributions to Mineralogy and Petrology 158, 485-504.

McCanta, M.C., Beckett, J.R., Stolper, E.M. (2008). Zonation of phosphorus in olivine: Dynamic crystallization experiments and a study of chondrule olivine in unequilibrated ordinary chondrites. Lunar and Planetary Science XXXIX, 1807.

McCanta, M.C., Beckett, J.R., Stolper, E.M. (2009). Phosphorus zonation in H chondrite olivines: The effects of increasing petrologic grade. 40th lunar and planetary science conference, 2048.

Millman-Barris, M.S., Beckett, J.R., Baker, M.B., Hofmann, A.E., Morgan, Z., Crowley, M.R., Vielzeuf, D., Stolper, E. (2008). Zoning of phosphorus in igneous olivine. Contributions to Mineralogy and Petrology 155, 739-765.

Mysen B.O. and Virgo D. (1980) Trace element partitioning and melt structure: an experimental study at 1 atm pressure. Geochimica et Cosmochimica Acta 44, 1917-1930.

Ohtani, E., Kawabe, I., Moriyama, J., Nagata, Y. (1989). Partitioning of elements between majorite garnet and melt and implications for petrogenesis of komatiite. Contributions to Mineralogy and Petrology, 103, 263-269.

Pack, A., Palme, H. (2003). Partitioning of Ca and Al between forsterite and silicate melt in dynamic systems with implications for the origin of Ca, Al-rich forsterite in primitive meteorites. Meteoritics and Planetary Science, 38, 1263-1281.

Pan, Y., Dong, P., Chen, N. (2003) Non-Henry's Law behavior of REE partitioning between fluorapatite and $CaF_2$-rich melts: Controls of intrinsic vacancies and implications for natural apatites. Geochimica et Cosmochimica Acta, 67, 1889-1900.

Prowatke, S., Klemme, S. (2006) Rare earth element partitioning between titanite and silicate melts: Henry's law revisited. Geochimica et Cosmochimica Acta, 70, 4997-5012.

Reitano, R., Smith, P.M., Aziz M.J. (1994). Solute trapping of group III, IV, and V elements in silicon by an aperiodic stepwise growth mechanism. Journal of Applied Physics 76, 1518-1529.

Schairer, J.F., Yoder, H.S. (1966). The system albite-anorthite-forsterite at 1 atmosphere. Carnegie Institute Washington, Yearbook 65, 206.

Spandler, C., O'Neill, H.St.C., Kamenetsky, V.S. (2007). Survival times of anomalous melt inclusions from element diffusion in olivine and chromite. Nature, 447, 303-306.

Toplis, M.J. and Corgne, A. (2002) An experimental study of element partitioning between magnetite, clinopyroxene and iron-bearing silicate liquids with particular emphasis on vanadium. Contributions to Mineralogy and Petrology. 144, 22-37.

Toplis, M.J., Libourel, G., Carroll, M.R. (1994). The role of phosphorus in crystallization processes of basalt: An experimental study. Geochimica et Cosmochimica Acta, 58, 797-810.

Tropper, P., Recheis, A., Konzett, J. (2004). Pyrometamorphic formation of phosphorus-rich olivines in partially molten metapelitic gneisses from a prehistoric sacrificial burning site (Otz Valley, Tyrol, Austria). European Journal of Mineralogy 16, 631-640.

Watson, E.B. (1977). Partitioning of manganese between forsterite and silicate liquid. Geochimica et Cosmochimica Acta, 41, 1363-1374.

Watson, E.B. (1979). Apatite saturation in basic to intermediate magmas. Geophysical Research Letters, 6, 937-940.

Welch, J.H. and Gutt, W. (1961) High temperature studies of the system calcium oxide – phosphorus pentoxide. Journal of the Chemical Society 4442-4444

Wolf, M.B. and London, D. (1994). Apatite dissolution into peraluminous haplogranitic melts: An experimental study of solubilities and mechanisms Geochimica et Cosmochimica Acta, 58, 4127-4145.

Witt-Eickschen, G., O'Neill, H.St.C. (2005). The effect of temperature on the equilibrium distribution of trace elements between clinopyroxene, orthopyroxene, olivine and spinel in upper mantle peridotite. Chemical Geology 221, 65-101.

**List of Tables.**

Table 1. Summary of previously reported olivine/melt partition coefficients for phosphorus.

Table 2. Chemical compositions of starting materials.

Table 3. Temperature conditions and durations of experiments.

Table 4. Compositions of olivines and coexisting glasses, together with calculated partition coefficients.

**Figure Captions.**

Figure 1. Compositions of starting materials and experimentally produced glasses expressed as a proportion of the number of Mg, Na and Ca cations. The filled symbols are starting materials and the open symbols are the melt compositions for samples 1-10 which were cooled at 1°C per hour to a final temperature of 1400°C (circles) or 1270°C (squares). In all cases the bulk compositions lie close to the tie line connecting the melt compositions with the Mg apex (as expected if forsterite is the only crystalline phase).

Figure 2. Examples of P zoning profiles in experimentally produced olivines. Each panel shows the profiles for several crystals from a specific sample. To aid comparison, all profiles represent crystallization from starting material 3. Panels A, B and C all show crystals from the series of experiments cooled to a temperature of 1400°C. Note the relatively constant P concentration and similarity between the 3 crystals in A (1°C/hour), and the more varied style of zoning and absolute P concentrations in B and C (5°C and 10°C/hour respectively). D shows the data for 3 crystals in a sample cooled at 1°C/hour to 1270°C. Despite the much higher P concentrations in the olivine, all 3 crystals have similar zoning profiles and similar absolute P concentrations.

Figure 3. The chemical gradients at an olivine-melt interface in sample 2 elucidated by FEG EPMA. (a) is a back-scattered electron image, (b) and (c) are X-ray maps of Mg and Si respectively, (d) is a P X-ray map obtained by summing the output of 3 different

642 spectrometers, and (e) is a traverse generated using imagej64 to integrate the count rates for
643 rectangular area shown in (d). Note the rise and then fall in the P count rate from core to rim
644 within the olivine, the sharp transition from olivine to glass and the homogeneous nature of
645 the glass adjacent to the crystal. The field of view in (a) to (d) is 61.4 x 61.4 μm and the pixel
646 size is 0.12 x 0.12 μm.
647
648 Figure 4. A high-resolution line scan across an olivine crystal in sample 6, the sample with
649 the highest partition coefficient in this study, and hence the sample most likely to display
650 non-equilibrium features. (a) shows a BSE image of the crystal oriented so that the traverse
651 runs horizontally from west to east. The scale bar is 100 microns. (b) shows wt% $P_2O_5$
652 concentration (black squares) across the whole crystal together with wt% $SiO_2$/50 (red
653 diamonds) to clearly show the boundary between olivine and glass. (c) is a close-up view of
654 the edge of the crystal, showing that the complex excursions in $P_2O_5$ concentration occur
655 within the olivine.
656
657 Figure 5. Correlations between P concentration and concentration of other elements in
658 olivine, where concentrations are expressed as the number of cations per four oxygens. Data
659 points are for samples 1-10, which were all cooled at 1°C/hour. The solid lines are not fits to
660 the data, they are the predicted co-variations of elemental abundances for reactions (1), (2),
661 and (3). The slopes strongly support equation (1) as the correct mechanism for P
662 incorporation in olivine in this study. The 1% offset between experiment and prediction
663 (discussed in the text) for Si and Mg is almost certainly an analytical artifact.
664
665 Figure 6. Phosphorus partition coefficients for all samples plotted as a function of NBO/T
666 and $X_{SiO2}$. Error bars are smaller than the symbols unless shown. The samples with cooling
667 rates of 1°C/hour are plotted with filled symbols. Circles are samples 6-10 (cooled to
668 1270°C), squares are samples 1-5 (cooled to 1400°C) and diamonds are samples 21-23
669 (cooled to 1400°C but with varying bulk P concentration). The samples with more rapid
670 cooling rates are plotted with open or grey symbols. The open triangles are samples 17-20
671 (5°C/hour), the grey triangles are samples 24-28 (10°C/hour). Three methods were initially
672 used for the calculation of NBO/T. In all cases, the first step is to recalculate melt
673 compositions in terms of number of cations per 100 oxygens. In method one, it is assumed
674 that P polymerises the melt, so the number of NBO is calculated as 2(Mg+Ca)+Na-Al

675 (because some cations are removed from a network modifying role by charge balancing
676 tetrahedral Al) and T is (Si+Al+P). In method 2, it is assumed that P depolymerises the melt
677 (while remaining tetrahedrally coordinated), so NBO is calculated as 2(Mg+Ca)+Na+P-Al
678 and T is (Si+Al+P). As we do not know which of these models is correct (and there is very
679 little difference in the calculated value of NBO/T anyway) the value used here is the average
680 of the two calculations. A third method simply uses the equation NBO/T = [200-
681 4(Si+Al+P)]/[Si+Al+P], and gives essentially the same as method 2 in this simple system.
682 $X_{SiO2}$ was calculated on a single-cation basis, e.g. using $X_{AlO1.5}$ not $X_{Al2O3}$ (following Evans et
683 al., 2008). The lines through the data are least squares linear fits through the 1°C/hour data
684 only.
685
686

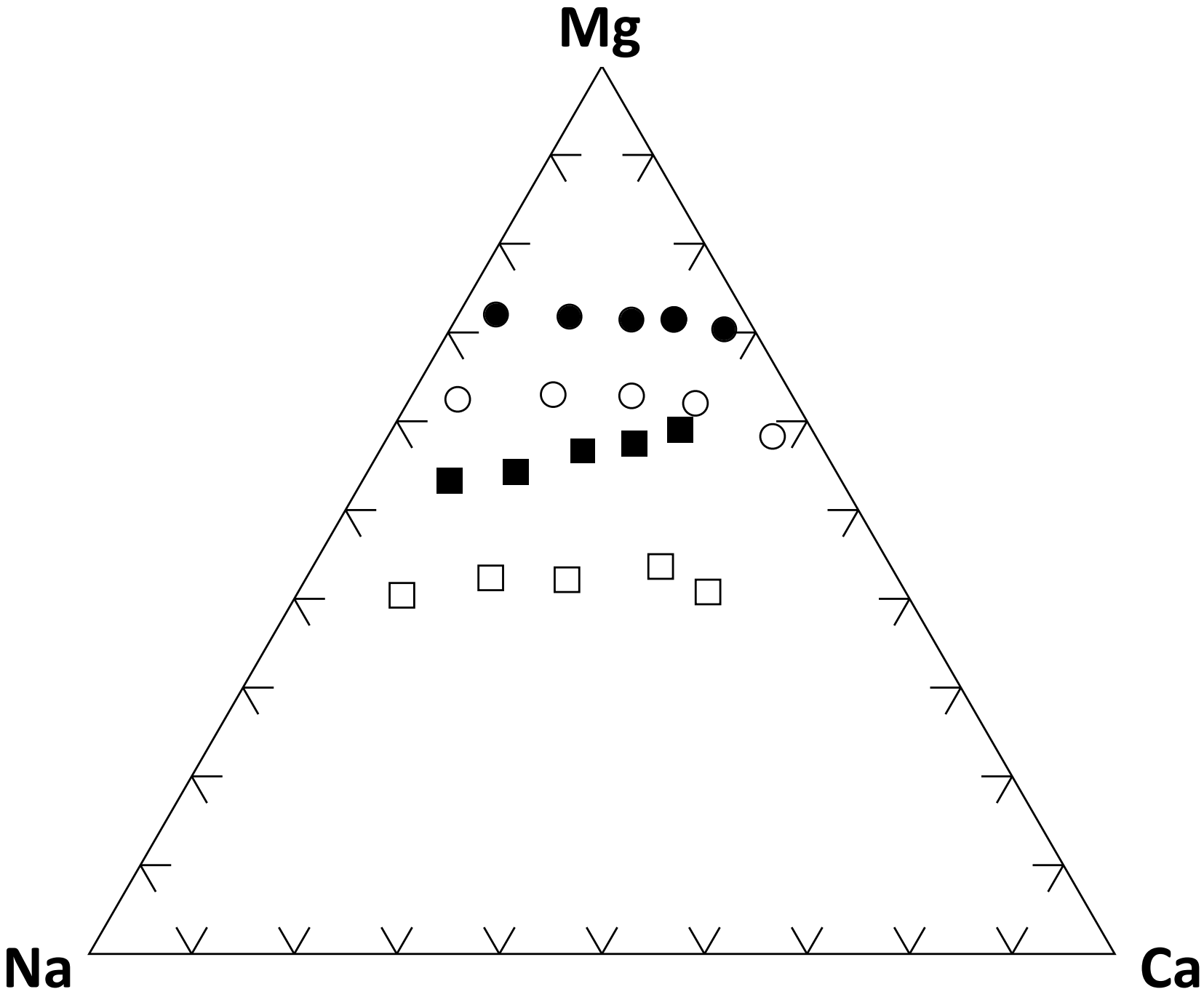
Mg
Na
Ca

This is a preprint, the final version is subject to change, of the American Mineralogist (MSA)
Cite as Authors (Year) Title. American Mineralogist, in press.
(DOI will not work until issue is live.) DOI: http://dx.doi.org/10.2138/am.2013.4237


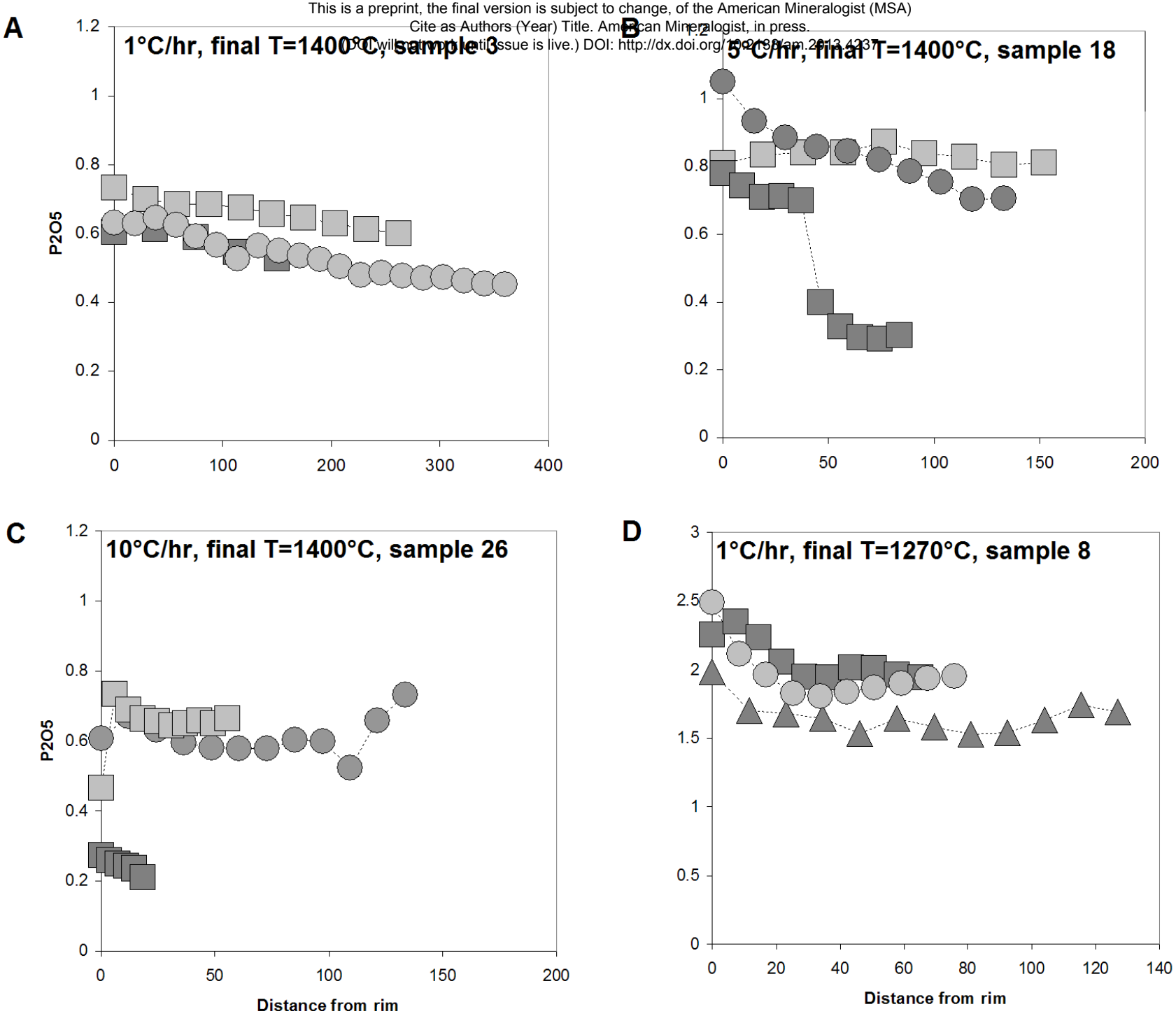

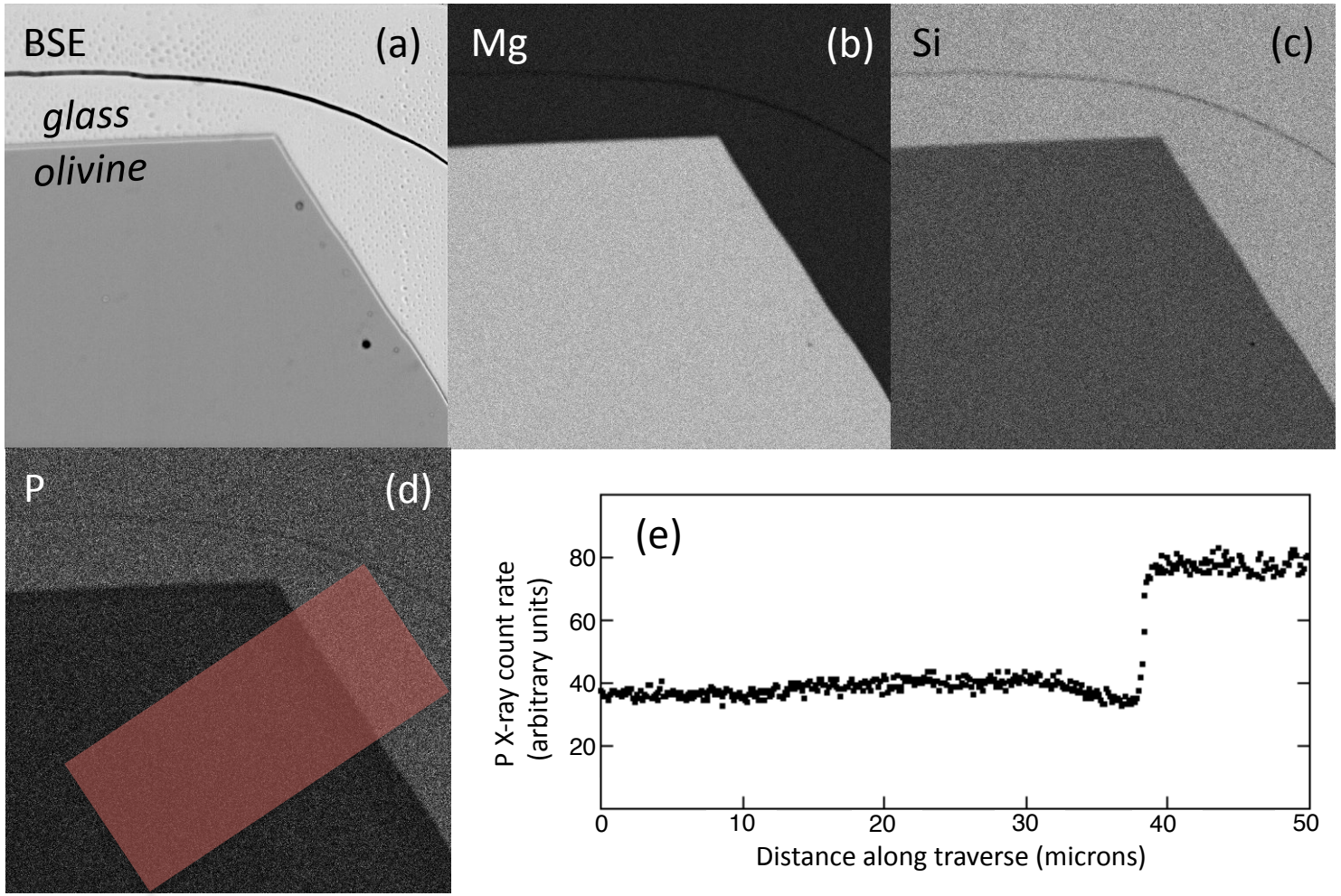
BSE
(a)
glass
olivine
Mg
(b)
Si
(c)
P
(d)
(e)
P X-ray count rate
(arbitrary units)
80
60
40
20
0
10
20
30
40
50
Distance along traverse (microns)

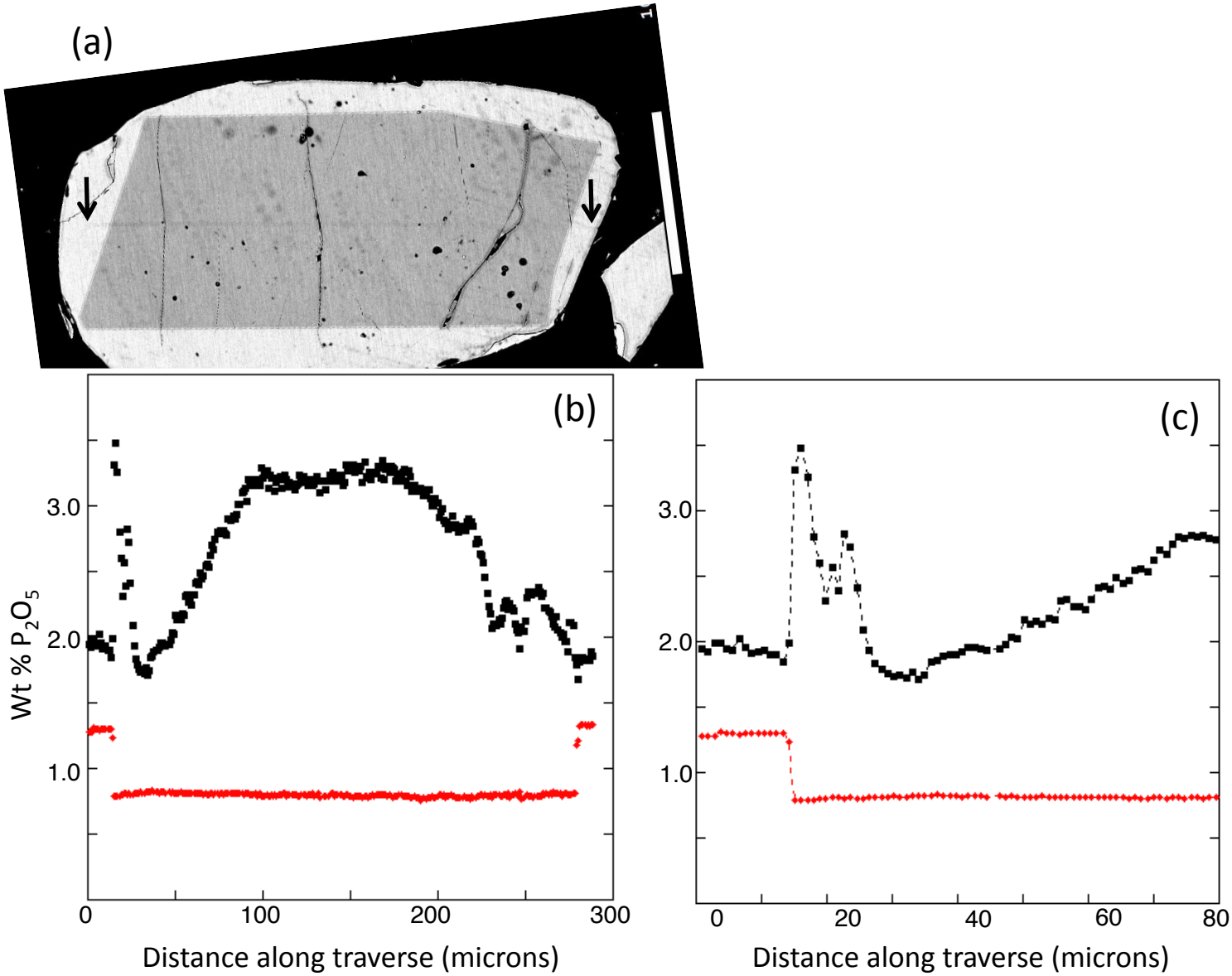
(a)
(b)
(c)
Wt % $P_2O_5$
3.0
2.0
1.0
0
100
200
300
Distance along traverse (microns)
3.0
2.0
1.0
0
20
40
60
80
Distance along traverse (microns)

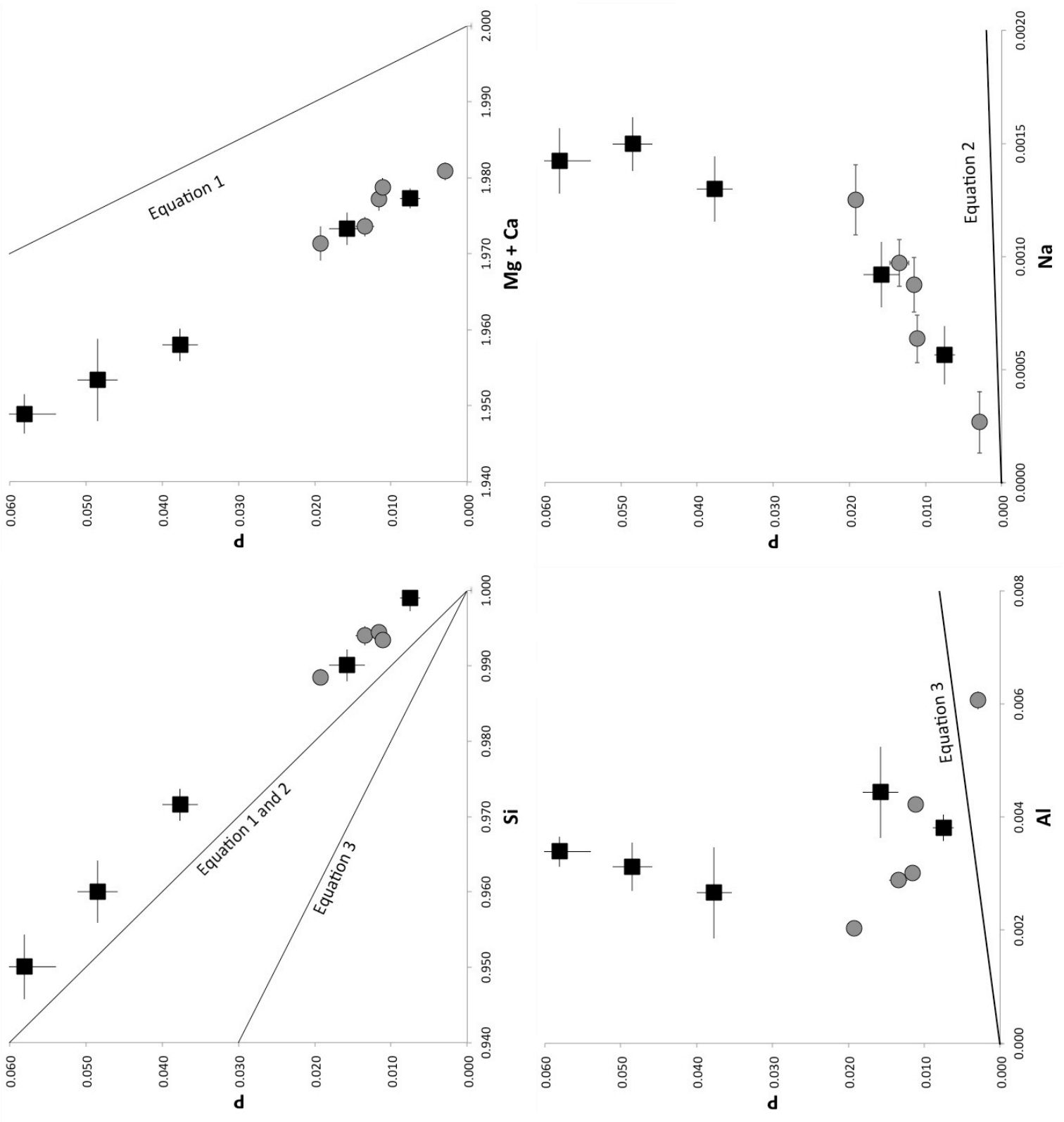
Equation 1
Mg + Ca
Equation 2
Na
Equation 1 and 2
Equation 3
Si
Equation 3
Al
Pd

Figure 6

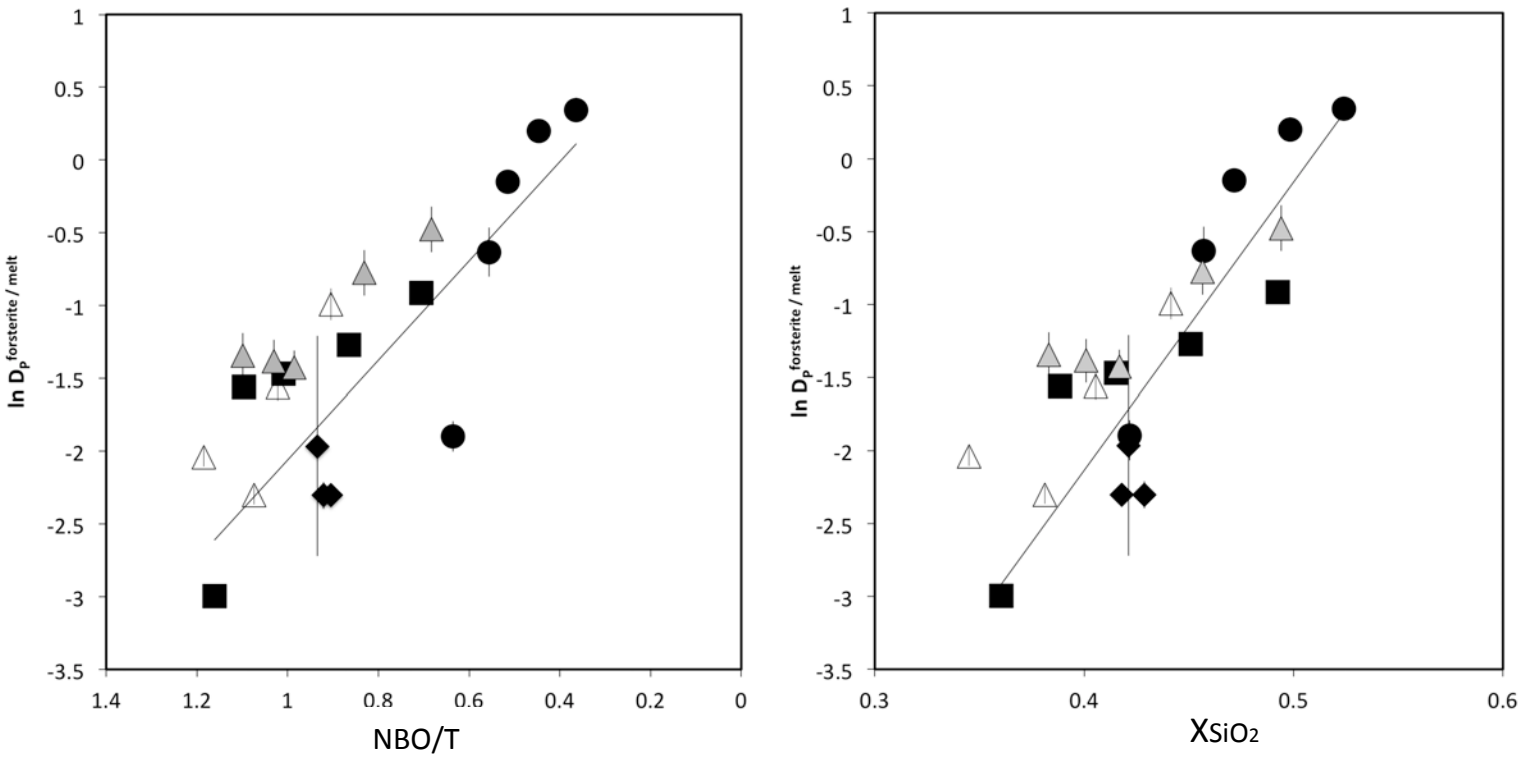

Table 1. Summary of previously reported olivine/melt partition coefficients for phosphorus.

| Rock Type | $D_P^{ol/melt}$ | Reference |
|---|---|---|
| **Experimental studies** | | |
| nepheline basanite | 0.038-0.05 | 1 |
| nepheline basanite | 0.05 | 1 |
| Mauna Kea basalt (doped) | 0.5-<0.1 | 2 |
| ferro-basalt | 0.02-0.2 | 3 |
| **Natural mineral-melt pairs** | | |
| subalkaline basalt | 0.043 | 4 |
| subalkaline andesite | 0.055 | 4 |
| alkaline basalt | 0.019 | 4 |
| chassignite | 0.3 | 5 |
| spinel lherzolite | 0.1 | 6 |
| ugandite / leucite basanite | 0.01-.02 | 7 |

1) Adam and Green (2006)

2) Millman-Barris et al. (2008)

3) Toplis et al. (1994)

4) Anderson and Greenland (1969)

5) Beck et al. (2006)

6) Brunet and Chazot (2001)

7) Foley et al. (2011)

Table 2. Chemical compositions of starting materials.

| | composition number | | | | | | | | | | | | |
|---|---|---|---|---|---|---|---|---|---|---|---|---|---|
| Oxide Wt. % | 1 | 2 | 3 | 4 | 5 | 6 | 7 | 8 | 9 | 10 | 11 | 12 | 13 |
| MgO | 23.92 | 25.27 | 26.4 | 27.41 | 27.89 | 14.05 | 14.99 | 16.92 | 17.97 | 19.46 | 28.43 | 29.25 | 30.11 |
| $SiO_2$ | 54.33 | 49.87 | 45.74 | 42.59 | 38.82 | 57.31 | 53.96 | 50.63 | 47.69 | 44.59 | 45.34 | 45.03 | 44.69 |
| $Al_2O_3$ | 11.85 | 12.83 | 13.8 | 14.46 | 15.64 | 15.76 | 16.39 | 16.79 | 17.37 | 17.76 | 13.69 | 13.59 | 13.49 |
| $P_2O_5$ | 2.00 | 2.00 | 2.00 | 2.02 | 2.02 | 2.01 | 2.03 | 2.02 | 2.00 | 2.03 | 0.97 | 0.64 | 0.31 |
| CaO | 1.69 | 5.36 | 8.81 | 11.36 | 14.76 | 3.12 | 5.98 | 8.24 | 10.6 | 12.89 | 8.26 | 8.20 | 8.14 |
| $Na_2O$ | 6.21 | 4.67 | 3.24 | 2.15 | 0.88 | 7.76 | 6.64 | 5.40 | 4.36 | 3.26 | 3.30 | 3.28 | 3.26 |

Table 3. Temperature/time conditions of experiments.

| Sample no. | Starting material | Run temperature °C | Ramp °/hr | Initial dwell time (hr) | Final dwell time (hr) | Total run time (hr) |
|---|---|---|---|---|---|---|
| 1 | 1 | 1530-1400 | 1 | 5 | 2 | 137 |
| 2 | 2 | 1530-1400 | 1 | 5 | 2 | 137 |
| 3 | 3 | 1530-1400 | 1 | 5 | 2 | 137 |
| 4 | 4 | 1530-1400 | 1 | 5 | 2 | 137 |
| 5 | 5 | 1530-1400 | 1 | 5 | 2 | 137 |
| 6 | 6 | 1400-1270 | 1 | 5.3 | 3 | 138.3 |
| 7 | 7 | 1400-1270 | 1 | 5.3 | 3 | 138.3 |
| 8 | 8 | 1400-1270 | 1 | 5.3 | 3 | 138.3 |
| 9 | 9 | 1400-1270 | 1 | 5.3 | 3 | 138.3 |
| 10 | 10 | 1400-1270 | 1 | 5.3 | 3 | 138.3 |
| 17 | 2 | 1530-1400 | 5 | 0 | 0 | 26 |
| 18 | 3 | 1530-1400 | 5 | 0 | 0 | 26 |
| 19 | 4 | 1530-1400 | 5 | 0 | 0 | 26 |
| 20 | 5 | 1530-1400 | 5 | 0 | 0 | 26 |
| 21 | 11 | 1530-1400 | 1 | 0 | 11.5 | 141.5 |
| 22 | 12 | 1530-1400 | 1 | 0 | 11.5 | 141.5 |
| 23 | 13 | 1530-1400 | 1 | 0 | 11.5 | 141.5 |
| 24 | 1 | 1530-1400 | 10 | 0 | 4 | 17 |
| 25 | 2 | 1530-1400 | 10 | 0 | 4 | 17 |
| 26 | 3 | 1530-1400 | 10 | 0 | 4 | 17 |
| 27 | 4 | 1530-1400 | 10 | 0 | 4 | 17 |
| 28 | 5 | 1530-1400 | 10 | 0 | 4 | 17 |

Table 4. Compositions of olivines and coexisting glasses, together with calculated phosphorus partition coefficients ($D_P$). All compositions expressed as wt%. The standard deviation (given in parentheses) is calculated from the spread of compositions across all analysed points. It is dominated by heterogeneity in the samples rather than counting statistics of EMPA. See text for calculation of NBO/T.

| | MgO | $SiO_2$ | $Al_2O_3$ | $P_2O_5$ | CaO | $Na_2O$ | Total | N[a] | | |
|---|---|---|---|---|---|---|---|---|---|---|
| Olivine compositions | | | | | | | | | | |
| 1 | 56.01(16) | 41.89(22) | 0.073(2) | 0.961(73) | 0.044(2) | 0.027(7) | 99.00 | 20 | | |
| 2 | 55.81(12) | 41.98(12) | 0.103(8) | 0.670(123) | 0.139(4) | 0.021(5) | 98.73 | 20 | | |
| 3 | 55.89(9) | 42.04(9) | 0.108(3) | 0.576(79) | 0.247(5) | 0.019(5) | 98.87 | 35 | | |
| 4 | 55.86(17) | 42.01(14) | 0.151(6) | 0.555(72) | 0.364(5) | 0.014(5) | 98.96 | 20 | | |
| 5 | 56.20(24) | 42.67(23) | 0.219(11) | 0.146(7) | 0.598(17) | 0.006(6) | 99.84 | 20 | | |
| 6 | 55.25(15) | 40.20(33) | 0.121(19) | 2.896(418) | 0.087(5) | 0.031(6) | 98.58 | 43 | | |
| 7 | 55.93(28) | 40.98(25) | 0.114(32) | 2.453(272) | 0.147(5) | 0.033(5) | 99.66 | 42 | | |
| 8 | 55.50(17) | 41.16(15) | 0.096(7) | 1.885(240) | 0.201(8) | 0.028(6) | 98.88 | 34 | | |
| 9 | 56.13(19) | 42.12(17) | 0.160(58) | 0.792(237) | 0.262(10) | 0.020(6) | 99.49 | 38 | | |
| 10 | 55.87(19) | 42.27(13) | 0.137(17) | 0.374(136) | 0.356(8) | 0.012(6) | 99.02 | 24 | | |
| 17 | 57.28(26) | 41.72(30) | 0.087(8) | 1.171(340) | 0.134(6) | 0.029(4) | 100.42 | 27 | | |
| 18 | 57.68(15) | 41.65(16) | 0.115(9) | 0.731(203) | 0.247(11) | 0.023(5) | 100.45 | 30 | | |
| 19 | 57.09(82) | 42.19(28) | 0.142(20) | 0.380(102) | 0.361(11) | 0.015(5) | 100.19 | 26 | | |
| 20 | 57.14(85) | 42.09(35) | 0.270(103) | 0.513(125) | 0.305(52) | 0.009(6) | 100.32 | 29 | | |
| 21 | 57.41(39) | 42.87(37) | 0.114(22) | 0.186(51) | 0.270(15) | 0.015(5) | 100.86 | 73 | | |
| 22 | 58.02(23) | 42.79(16) | 0.116(10) | 0.070(8) | 0.276(6) | 0.007(3) | 101.28 | 86 | | |
| 23 | 57.54(21) | 42.97(14) | 0.118(9) | 0.039(7) | 0.333(15) | 0.009(4) | 101.02 | 41 | | |
| 24 | 57.45(19) | 41.33(56) | 0.207(53) | 1.384(728) | 0.171(174) | 0.030(16) | 100.58 | 38 | | |
| 25 | 56.89(15) | 41.67(35) | 0.140(19) | 1.049(458) | 0.143(54) | 0.034(16) | 99.93 | 32 | | |
| 26 | 57.02(20) | 41.92(20) | 0.179(43) | 0.512(164) | 0.250(11) | 0.020(6) | 99.90 | 37 | | |
| 27 | 56.56(43) | 42.10(33) | 0.266(129 | 0.394(94) | 0.391(157) | 0.012(5) | 99.72 | 31 | | |
| 28 | 56.37(199) | 41.74(57) | - | 0.393(174) | - | - | 98.50 | 24 | | |
| Glass compositions | | | | | | | | | NBO/T | $D_P$ |
| 1 | 17.23(41) | 57.62(41) | 13.78(31) | 2.38(12) | 1.80(4) | 6.96(31) | 99.77 | 20 | 0.705 | 0.40(4) |
| 2 | 18.83(31) | 52.52(52) | 14.84(34) | 2.40(9) | 5.72(6) | 5.34(20) | 99.64 | 23 | 0.865 | 0.28(5) |
| 3 | 19.99(29) | 48.42(31) | 15.80(23) | 2.55(12) | 9.50(12) | 3.83(15) | 100.08 | 17 | 1.009 | 0.23(3) |
| 4 | 20.20(32) | 44.90(36) | 16.88(34) | 2.70(11) | 12.73(7) | 2.47(11) | 99.88 | 20 | 1.096 | 0.21(3) |
| 5 | 19.26(28) | 41.34(40) | 18.40(34) | 2.87(10) | 17.24(13) | 1.07(12) | 100.18 | 25 | 1.161 | 0.051(3) |
| 6 | 8.85(186) | 60.14(134) | 17.15(73) | 2.05(20) | 3.14(42) | 8.31(54) | 99.64 | 26 | 0.364 | 1.41(25) |
| 7 | 9.89(58) | 57.17(55) | 17.86(38) | 2.01(21) | 5.84(14) | 7.12(21) | 99.96 | 25 | 0.446 | 1.22(19) |
| 8 | 10.34(26) | 54.01(51) | 18.73(30) | 2.20(14) | 8.70(10) | 6.10(16) | 100.09 | 25 | 0.515 | 0.86(12) |
| 9 | 10.77(31) | 51.79(80) | 19.89(40) | 1.49(60) | 11.65(20) | 4.26(55) | 99.85 | 25 | 0.556 | 0.53(27) |
| 10 | 10.63(22) | 47.61(52) | 20.61(33) | 2.52(13) | 14.50(9) | 3.86(21) | 99.72 | 20 | 0.635 | 0.15(6) |
| 17 | 19.41(71) | 51.77(29) | 14.63(22) | 3.18(16) | 5.81(7) | 5.36(15) | 100.15 | 13 | 0.904 | 0.37(11) |
| 18 | 19.62(21) | 47.16(38) | 15.80(24) | 3.56(17) | 9.90(11) | 3.94(25) | 99.99 | 16 | 1.021 | 0.21(6) |
| 19 | 19.46(19) | 44.27(46) | 17.27(24) | 3.76(21) | 13.29(13) | 2.62(16) | 100.67 | 14 | 1.074 | 0.10(3) |
| 20 | 19.33(29) | 39.83(42) | 18.86(22) | 3.89(12) | 17.84(21) | 1.13(10) | 100.87 | 16 | 1.185 | 0.13(3) |
| 21 | 18.59(24) | 49.29(35) | 16.97(16) | 1.29(7) | 10.09(7) | 4.19(11) | 100.42 | 27 | 0.934 | 0.14(4) |
| 22 | 19.26(91) | 49.68(80) | 17.24(16) | 0.70(27) | 10.31(22) | 2.84(105) | 100.02 | 32 | 0.921 | 0.10(4) |
| 23 | 17.80(16) | 48.94(75) | 17.92(16) | 0.41(2) | 10.65(12) | 4.52(13) | 100.22 | 20 | 0.905 | 0.10(2) |
| 24 | 16.55(57) | 57.44(48) | 13.92(23) | 2.23(12) | 1.83(5) | 7.16(26) | 99.12 | 24 | 0.683 | 0.62(33) |
| 25 | 18.09(19) | 52.84(55) | 14.86(23) | 2.27(11) | 5.77(6) | 5.32(24) | 99.15 | 13 | 0.831 | 0.46(20) |
| 26 | 19.39(38) | 47.97(34) | 16.01(23) | 2.14(21) | 9.56(11) | 3.77(17) | 98.83 | 18 | 0.985 | 0.24(8) |
| 27 | 19.64(29) | 45.81(81) | 17.50(36) | 1.55(56) | 13.08(25) | 1.66(81) | 99.24 | 29 | 1.030 | 0.25(11) |
| 28 | 19.81(35) | 43.46(37) | 18.04(24) | 1.49(7) | 15.08(8) | 0.91(11) | 98.78 | 29 | 1.099 | 0.26(12) |

[a]N is the number of analyses.